IFSCC 2025 full paper (IFSCC2025-614)

"Next-Generation Madecassoside-Functionalized Platinum Liposomes: A Super-Molecular Approach for Rapid Soothing and Long-Term Homeostasis of Sensitive Skin"

Jing Sun [1], Yongjie Lu [1], Dongying Zhang [1], Lu Ren [1], Shuangyan Wang [1], Yanhong Liu [1], Xiaozhi Wang [1],Zhiting Zhang [1], Qipeng Lu [2], Li Ye [3,4], Yan Huang [5], Tomoko Oto [6], Naisheng Jiang [2,*] and Dongcui Li [1,*]

[1] Research and Development, Hua An Tang Biotech Group Co., Ltd., Guangzhou, China;
[2] Key Laboratory of Advanced Materials and Devices for Post-Moore Chips, Ministry of Education, School of Materials Science and Engineering, University of Science and Technology Beijing, Beijing, China;
[3] Dermatology Hospital, Southern Medical University, Guangzhou, Guangdong, China;
[4] Hygiene Detection Center,School of Public Health, Southern Medical University (NMPA Key Laboratory for Safety Evaluation of Cosmetics, Guangdong Provincial Key Laboratory of Tropical Disease Research), Guangzhou, China;
[5] Key Laboratory for Analytical Science of Food Safety and Biology, Ministry of Education, College of Biological Science & Engineering, Fuzhou University, Fuzhou, China;
[6] Nihon Inemoto Co., Ltd., Tokyo, Japan

1. Introduction

The skin serves as the primary defense against environmental assaults; however, chronic irritation can compromise this barrier, leading to heightened discomfort due to inflammation and hypersensitivity, particularly common in sensitive skin [1]. Characterized by an exaggerated response to environmental stimuli, sensitive skin frequently manifests symptoms such as burning, tingling, itching, and tightness, often accompanied by erythema or scaling [2]. The underlying pathophysiology of sensitive skin involves a combination of impaired skin barrier function, enhanced neurovascular reactivity, and amplified immune-inflammatory responses [3]. A compromised skin barrier exposes nerve endings to external stimuli, which activates specific receptors such as endothelin A receptor (ETRA), transient receptor potential vanilloid 1 (TRPV1), and transient receptor potential ankyrin 1 (TRPA1) [4]. This activation, in turn, leads to the release of neuropeptides such as substance P and calcitonin gene-related peptide, which bind to neurokinin 1 receptors (NK1R), promote calcium influx and initiate an inflammatory response [5]. Moreover, the histamine H1 receptor (H1R) plays a crucial role in mediating histamine-induced pruritus by promoting calcium influx and transmitting itch signals [6]. These interconnected mechanisms can lead to a vicious cycle of barrier dysfunction, resulting in localized

redness, swelling, heat, pain, and itching [7]. Therefore, novel formulations that address both inflammation and neurogenic pathways are urgently needed to improve therapeutic outcomes for sensitive skin.

In this context, platinum (Pt) particles have drawn increasing interest in dermatology due to their antioxidant and anti-inflammatory properties, with several applications already approved for cosmetic use [8]. These properties make Pt particles potentially beneficial for alleviating skin irritation and minimizing adverse reactions in sensitive skin, making them especially suitable for sensitive skin [9-11]. While conventional Pt particles have shown improved performance, they are not specifically designed to meet the unique needs of sensitive skin care, particularly in providing rapid soothing and maintaining long-term homeostasis[12]. Their limited efficacy in regulating inflammatory and neurogenic pathways further restricts their application in cosmetics. To address this, Pt particles are often functionalized with organic or inorganic molecules—such as ligands, polymers, peptides, antibodies, or bioactive compounds—to improve their targeting ability, stability, and biomedical compatibility [13]. Such functionalization has been successfully applied in fields like oncology and infection control, where functionalized Pt particles can be engineered to target specific pathways, inducing apoptosis in cancer cells or combating pathogens [14-16]. This strategy presents a promising opportunity to improve Pt-based formulations for cosmetic applications as well, particularly in managing inflammation and neurogenic responses in sensitive skin.

Meanwhile, natural plant-derived active ingredients are increasingly valued in cosmetics for their safety, efficacy, and mild nature. Madecassoside (MAD), the most abundant triterpenoid compound extracted from Centella asiatica, has demonstrated diverse bioactivities including moisturizing, antioxidant, antibacterial, anti-inflammatory, and wound-healing effects [17]. Clinically, it has been widely used for treating infected wounds, burns, scalds, and hypertrophic scars, offering strong potential for use in sensitive skin care [18]. The extensive biological activity and potent skin care efficacy of MAD offer a promising solution for sensitive skin care.

In this study, we developed a novel platinum-based formulation incorporating MAD to specifically address the challenges of sensitive skin. AI-driven molecular docking simulations were employed to assess and compare the binding affinities of MAD-functionalized Pt (Pt-MAD) versus unmodified Pt particles on five key sensory receptors associated with skin sensitivity. Furthermore, Pt-MAD particles were also encapsulated within liposomes to enhance delivery efficiency and improve physicochemical stability, aiming to provide both immediate relief and long-term therapeutic benefits. In vitro experiments revealed that Pt-MAD liposomes significantly outperformed unmodified Pt particles in reducing inflammation and hypersensitivity. These findings suggest Pt-MAD liposomes as a promising next-generation therapeutic approach for sensitive skin, offering rapid soothing effects while promoting long-term skin health.

2. Materials and Methods

2.1. AI-Docking

Theoretical protein-ligand binding calculations were performed using the DynamicBind model, developed by Galixir Technologies, to compare the targeting capacities of Pt atoms and Pt-

MAD complex. DynamicBind is an advanced deep learning-based docking method that integrates geometric networks and a diffusion model to efficiently predict protein-ligand interactions[19]. This method accounts for significant protein conformational changes, including the identification of cryptic binding pockets, which are often difficult to detect with traditional docking techniques. One of the key advantages of DynamicBind is its ability to accurately predict ligand-specific conformations directly from unbound protein structures, eliminating the need for experimentally determined holo-structures. This tool enables rapid and relatively accurate docking results through its advanced algorithm. For this study, we selected five proteins associated with dermal sensory receptors (i.e., TRPV1, TRPA1, ETAR, H1R1, and NK1R) and used their structural data, along with ligand information for Pt and Pt-MAD, as input for the docking simulations. The simulations provided insights into the binding conformations and mechanisms of action of these complexes.

2.2. Physicochemical Characterization of Pt-MAD Liposomes

Pt and Pt-MAD supermolecules were synthesized and functionalized using an in-house patented process. Liposomes were prepared by encapsulating Pt or Pt-MAD using the thin-film hydration method. To confirm the successful modification of MAD with Pt, Fourier Transform Infrared Spectroscopy (FTIR) and Small-Angle X-ray Scattering (SAXS) analyses were performed, and results were compared with Pt-PVP, PVP, and MAD controls. The stability, dispersion, and particle size distribution of Pt and Pt-MAD liposome solutions were assessed using Dynamic Light Scattering (DLS). The solutions were diluted with ultrapure water to an appropriate concentration, placed in cuvettes, and measured using a Malvern Zetasizer Advance to determine the average particle size and polydispersity index (PDI).

2.3. Histamine-Induced Calcium Imaging Assay

Normal human epidermal keratinocytes (NHEK) were cultured in Eagle's Minimum Essential Medium (EMEM). Cells were seeded into 96-well culture plates and incubated for 24 hrs with loratadine as a positive control (PC). Prior to stimulation, the cells were pre-incubated with the test samples for 3 hrs. After removing the medium, the cells were incubated with Hank's Balanced Salt Solution (HBSS) containing Fluo-4 AM for 45 min at 37 °C. Following Fluo-4 AM loading, cells were washed five times with HBSS to remove excess dye. The cells were then pre-incubated with the test samples for an additional 30 min. Calcium imaging assays were performed using a Biotek Cytation Cell Imaging Multi-Mode Reader. After baseline kinetic data collection, 10 μM histamine was added to stimulate the cells, and the fluorescence intensity was measured after 1 min. The maximum relative fluorescence value was recorded and analyzed after 2 min of histamine stimulation.

2.4. TRPV1 Expression Assay

A suspension of NHEK cells was prepared and seeded into a 6-well plate. The cells were incubated for 24 hrs, after which the positive control (PC), capsazepine, and the test samples were pre-incubated with the cells for approximately 4 hrs. Following the incubation, the cells were washed and 2 mL of HBSS was added. The cells were then stimulated with 3 mJ UVB irradiation, after which the medium was replaced with fresh complete medium. The samples

were added again, and the cells were incubated for an additional 48 hrs for protein extraction. Protein concentration was determined using the Bicinchoninic Acid (BCA) Protein Quantification Kit. The protein was adjusted to a final concentration of 20 μg/20 μL and denatured at 95 °C for 10 min. A total of 20 μg of protein was loaded onto the gel and electrophoresis was performed. The gel was then transferred using a semi-dry transfer method. After transfer, the membrane was blocked with 5% skimmed milk at room temperature for 2 h. Following blocking, the membrane was washed three times with 0.1% Phosphate-Buffered Saline with Tween-20 (PBST), each wash lasting 5 min. The primary antibodies for TRPV1 (diluted 1:1000 in 0.1% PBST) and β-actin (diluted 1:1000) were incubated overnight at 4 °C. After incubation, the membrane was washed three times with PBST. The corresponding secondary antibody was diluted 1:10000 and incubated for 1 h, followed by three additional washes. Enhanced chemiluminescence (ECL) substrate was applied to the membrane for 1-2 min. Protein expression was detected using an imaging analyzer.

2.5. Pro-inflammatory Cytokine Expression

Fluorescence quantitative PCR (qPCR) was employed to assess the impact of the samples on the expression of pro-inflammatory cytokines following lipopolysaccharide (LPS)-induced stimulation in THP-1 cells. Cells were treated under optimal conditions, and total RNA was extracted using the Total Cellular RNA Extraction Kit. Complementary DNA (cDNA) was synthesized using the HiScript II Q RT SuperMix for qPCR (+gDNA wiper). After dilution, qPCR was conducted to measure the expression levels of TNF-α and IL-1β. PowerUp™ SYBR™ Green Master Mix was used to prepare the reaction mixture, and 0.1 μM primers for IL-8 and GAPDH were added to each reaction well. The primer sequences used for fluorescence quantitative PCR are listed in Table 1. The qPCR reactions were carried out using the Applied Biosystems QuantStudio 1 System with the standard qPCR program. The inhibition rate of gene expression was calculated using the following equation:

$$\text{Inhibition Ratio } (\%) = \frac{\text{MC-Sample}}{\text{MC-BC}} \times 100\%$$

Table 1. Fluorescence Quantitative PCR (qPCR) Primer Sequences.

Primer	Upstream sequence	Downstream sequence
TNF-α	5'-AGAACCCCGAGTGACAAGC-3'	5'-TGGGAGTAGATGAGGTACAGG-3'
IL-1β	5'-ATGCACCTGTACGATCACTG-3'	5'-ACAAAGGACATGGAGAACACC-3'
GAPDH	5'-GTCTCCTCTGACTTCAACAGCG-3'	5'-ACCACCCTGTTGCTGTAGCCAA-3'

2.6. Vasodilation Assay

Zebrafish were randomly distributed into 6-well plates with 15 fish per well. A zebrafish redness model was established by administering a high concentration of sodium lauryl sulfate (SLS) in water. Both a normal control group and a model control group were included. After incubation at 28 °C for 2 hrs, the high concentration-SLS was removed, and a lower concentration of SLS was maintained to continue the model. The samples were dissolved in water and added to the wells. After another 2-hour incubation, 10 zebrafish from each experimental group were selected and observed under a fluorescence microscope to monitor blood vessel changes. Image

analysis software was used to measure the average diameter of blood vessels at three points above the cloaca. The reduction effect of the samples on vasodilation was then calculated and evaluated. The Redness Reduction Effect was calculated using the following equation:

$$\text{Redness Reduction Effect (\%)} = \frac{\text{D(SLS)-D(sample)}}{\text{D(SLS)-D(control)}} \times 100\%$$

2.7. Inflammatory Factor IL-17 Expression

Zebrafish were randomly selected and distributed into 6-well plates with 30 fish per well. The zebrafish redness model was established by administering a high concentration of SLS in water. Three biological replicates were performed for each experimental condition. After incubation at 28 °C for 2 h, the high concentration of SLS was removed, and a lower concentration of SLS was maintained to continue the model. The samples were dissolved in water and added to the wells. After an additional 2-hour incubation, total RNA was extracted from zebrafish in each experimental group. cDNA was synthesized, and the expression of β-actin (as the internal reference) and the target gene IL-17 was measured using quantitative PCR (qPCR). The RNA relative expression of IL-17 was calculated by normalizing the expression of the target gene to the β-actin control, enabling comparison across experimental groups.

3. Results

3.1. AI-Docking

AI-driven docking simulations can provide detailed predictions of binding affinities, offering a more efficient and cost-effective approach to evaluating interactions at the molecular level. As shown in Figure 1, the Pt-MAD complex exhibited significantly stronger affinity for the five selected proteins (TRPV1, TRPA1, NK1R, H1R, ETAR) compared to the Pt atom alone. The MAD moiety in the Pt-MAD complex interacted effectively with the binding pockets of these proteins through hydrogen bonding and dipolar interactions. These interactions contributed to enhanced binding stability and molecular recognition, which are crucial for the improved targeting capabilities of Pt-MAD. The stronger and more stable binding of Pt-MAD to these sensory proteins suggests that Pt-MAD particles are more proficient in receptor targeting these receptors, potentially amplifying sensory-relieving activity and enhancing the efficacy of skin treatments through optimized protein interaction.

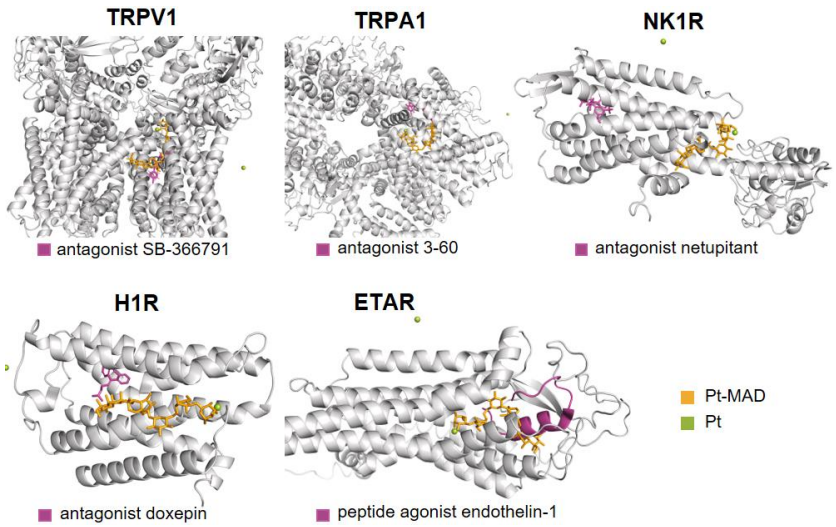

Figure 1. AI-driven molecular docking (Compound-Protein Interaction model) analysis of Pt atoms and the Pt-MAD complex targeting five key receptors(TRPV1, TRPA1, NK1R, H1R, and ETAR) associated with sensory responses in sensitive skin.

The Pt-MAD particles were encapsulated within liposomes to enhance their stability and facilitate transdermal delivery through the stratum corneum. As illustrated in Figure 2, this strategy enables that Pt-MAD can effectively penetrate the epidermal barrier. Upon reaching the deeper epidermal layers, the liposomal structure naturally dis-assembled, releasing Pt-MAD particles. The MAD moiety promotes effective binding to sensory receptor sites, thereby triggering the desired dermatological responses. Compared to unmodified Pt, Pt-MAD exhibits superior receptor-targeting capabilities. We postulate that the combination of MAD functionalization with liposome-mediated delivery optimizes the penetration and receptor-specific activity of Pt particles, which is crucial for targeted skin rejuvenation and repair.

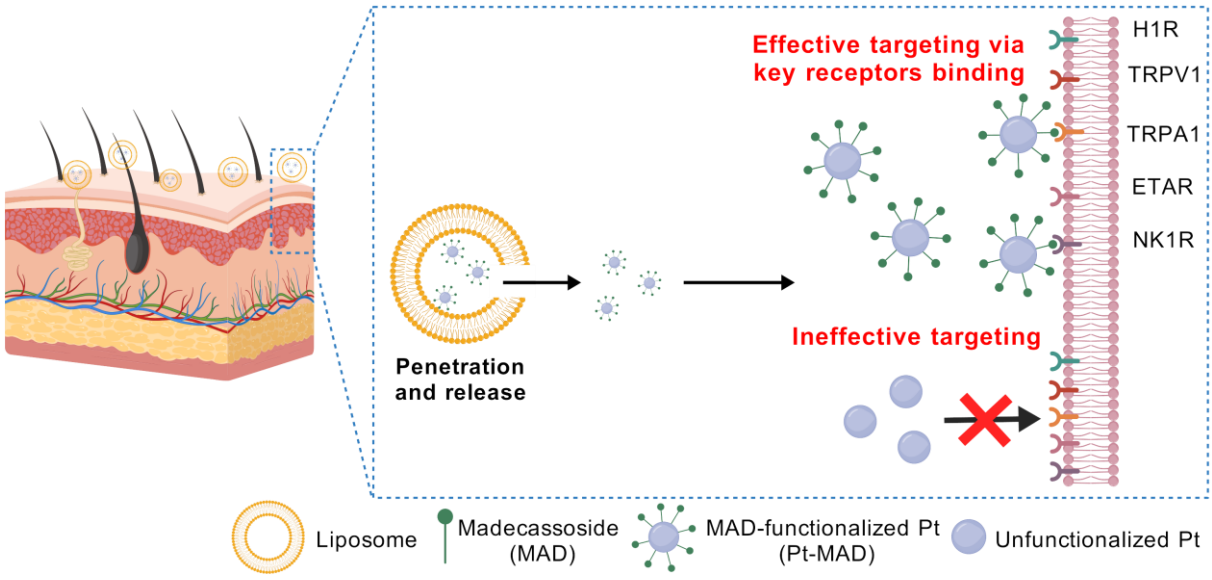

Figure 2. Schematic illustration of Pt-MAD liposomes, depicting their liposome-mediated transdermal delivery pathway and receptor-targeting mechanism.

3.2. Physicochemical Characterization of Pt-MAD Liposomes

As shown in Figure 3(a), the infrared spectrum of Pt-PVP exhibited characteristic peaks identical to those of PVP indicating that the Pt particles were fully capped with PVP. Upon functionalization with MAD, the infrared spectrum of Pt-MAD displayed two new distinct peaks, one around 3200~3500 cm^{-1} (corresponding to the O-H stretching vibration of the carboxyl group), and another near 1000 cm^{-1} (corresponding to the C-O stretching vibration of the ether group). These new peaks, absent in the Pt-PVP spectrum, are consistent with the MAD material, confirming successful conjugation of MAD to the Pt particles. From the SAXS curve in Figure 3(b), clear differences were observed between the Pt-MAD complex and the simple physical mixture, suggesting that a portion of MAD was not free but rather bound, further supporting the interaction between Pt and MAD. The combined SAXS and FTIR results indicate that Pt-MAD exists as a chemically integrated complex rather than a mere physical mixture. Figure 3(c) illustrates the schematic structure of the Pt-MAD liposomes in which Pt-MAD is encapsulated in the inner aqueous phase. The size distributions are shown in Figures 3(d). The average particle sizes of Pt liposomes and Pt-MAD liposomes are 147.6 nm and 159.2 nm, respectively, with PDI values of less than 0.1, indicating a uniform size for both liposomes.

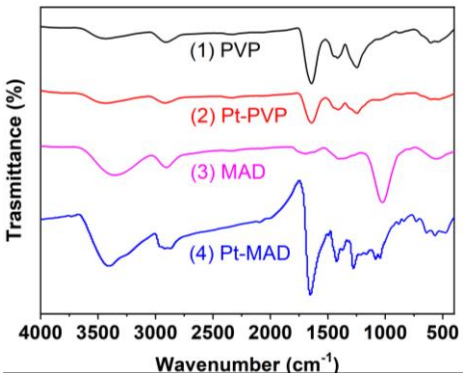

(a)

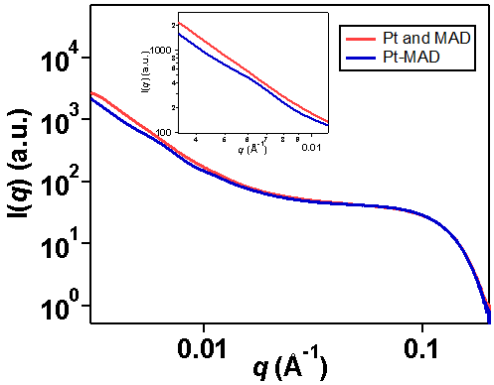

(b)

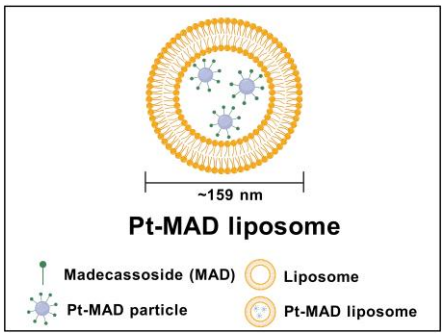

(c)

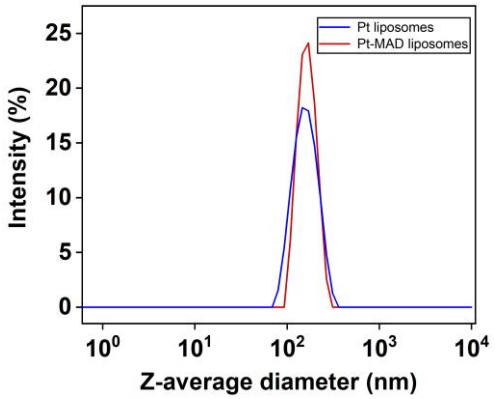

(d)

Figure 3. (a) Infrared absorption spectra of PVP, Pt-PVP, MAD, and Pt-MAD particles. (b) SAXS scattering intensity curves of the Pt-MAD complex and the physical mixture of Pt and MAD. (c) Schematic illustration of the structure of Pt-MAD liposomes. (d) Particle size distributions of Pt liposomes and Pt-MAD liposomes.

3.3. Histamine-Induced Calcium Imaging Assay

As shown in Figure 4(a), histamine stimulation led to an increase in intracellular Ca^{2+} levels in keratinocytes, confirming the successful establishment of the itch model. A lower relative fluores-cence intensity indicates a reduction in calcium ion concentration, reflecting a stronger ability to inhibit itching. Loratadine, a known antihistamine, was used as PC, and its fluorescence intensity decreased to levels comparable to the blank control (BC), confirming its strong antipruritic effect. The Pt and Pt-MAD liposomes also demonstrated significantly reduced intracellular calcium levels, with inhibition rates of 24.79% and 42.88%, respectively. Notably, Pt-MAD liposomes showed the highest inhibition rate, effectively reducing the itch response and mitigating further irritation and inflammation, as seen in Figure 4(b). These results suggest that Pt-MAD liposomes possess excellent antipruritic properties, and hold promise for therapeutic applications in histamine-induced itch conditions.

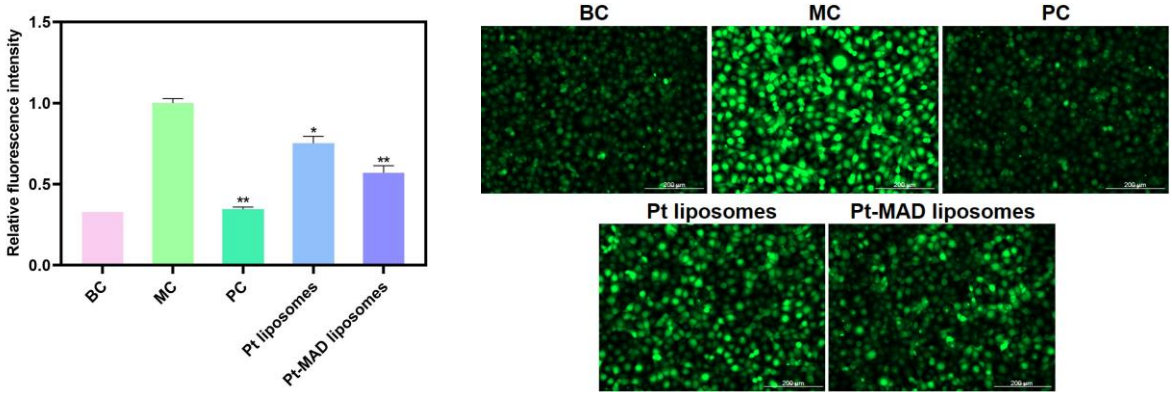

(a) (b)

Figure 4. Relative fluorescence intensity (a) and corresponding fluorescence microscopy images (b) of intracellular calcium levels in NHEK treated with blank control (BC), model control (MC; histamine), positive control (PC; loratadine), Pt liposomes, and Pt-MAD liposomes. The bar graph shows calcium concentration levels measured through kinetic detection after treatment. Data are expressed as mean ± SD from replicate experiments. *$p < 0.05$ and **$p < 0.01$ denote statistically significant differences compared to the MC group.

3.4. TRPV1 Expression Assay

TRPV1, commonly known as the capsaicin receptor, plays a critical role in modulating of pain and itch sensations [20]. Elevated expression of TRPV1 is often associated with enhanced sensory transmission and may contribute to skin hypersensitivity [21]. To evaluate the soothing effects of Pt and Pt-MAD liposomes, we examined their influence on TRPV1 protein expression. Western blot results, shown in Figure 5(a) and 5(b), revealed that UVB stimulation significantly upregulated TRPV1 expression. However, treatment with Pt liposomes and Pt-MAD liposomes resulted in a marked downregulation of TRPV1 expression in NHEK cells—by 36.2% and 66.0%, respectively, compared to the UVB control. Notably, Pt-MAD liposomes demonstrated a superior pain-relieving effect, as reflected by a greater reduction in gray density and a 7.8% improvement in chili flatness compared to PC. These findings suggest that Pt-MAD liposomes

exert their effect through the targeted interaction of MAD moieties with TRPV1 receptors, effectively alleviating pain and irritation.

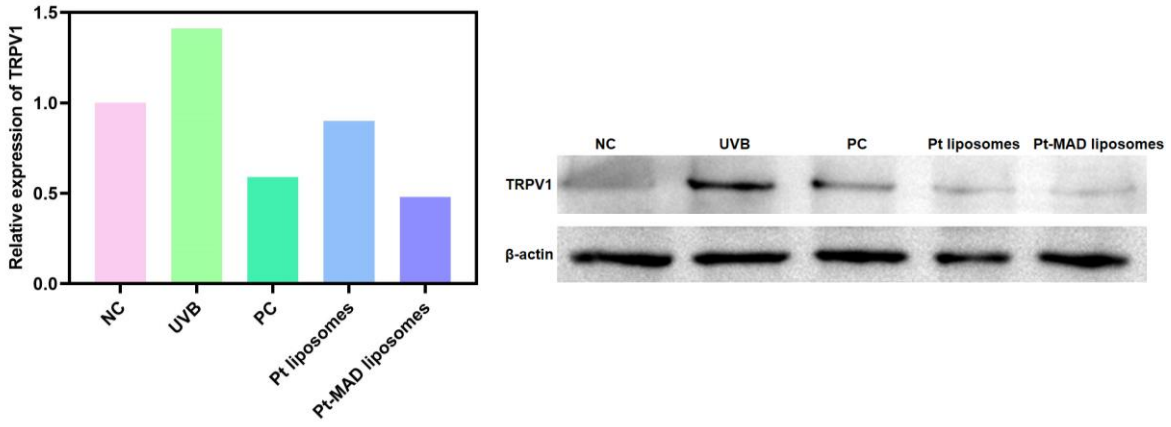

(a) (b)

Figure 5. Quantitative analysis (a) and representative Western blot images (b) of TRPV1 protein expression in NHEK cells treated with solvent control (negative control, NC), UVB control, capsaicin (PC), Pt liposomes, and Pt-MAD liposomes. The bar graph displays the relative expression levels of TRPV1 protein, as determined by Western blot analysis and grayscale quantification of protein bands.

3.5. Inflammatory Factor Expression Experiment

qPCR was employed to measure the relative expression of TNF-α and IL-1β mRNA in lipopolysaccharide (LPS)-stimulated THP-1 cells, to evaluate the inhibitory effect of Pt-based samples on the release of inflammatory factors. As shown in Figure 6, the elevated mRNA levels of TNF-α and IL-1β in the MC group confirmed the successful establishment of an inflammation model, relative to the baseline levels observed in the BC group. At a 0.4 ppm concentration, both Pt liposomes and Pt-MAD liposomes significantly reduced the relative expression of TNF-α and IL-1β mRNA compared to the model group. Specifically, Pt liposomes reduced TNF-α and IL-1β expression by 39.7% and 15.6%, respectively, while Pt-MAD liposomes achieved greater reductions of 66.9% and 23.6%, respectively. These results demonstrate that Pt-based samples effectively inhibit inflammatory factor expression. Notably, Pt-MAD liposomes exhibited a significantly stronger anti-inflammatory effect compared to Pt liposomes. The grafting of MAD enhanced the abil-ity of liposomes to directly target the inflammatory response pathway, thereby interrupting the pro-inflammatory cascade and delivering stronger anti-stress and anti-inflammatory benefits.

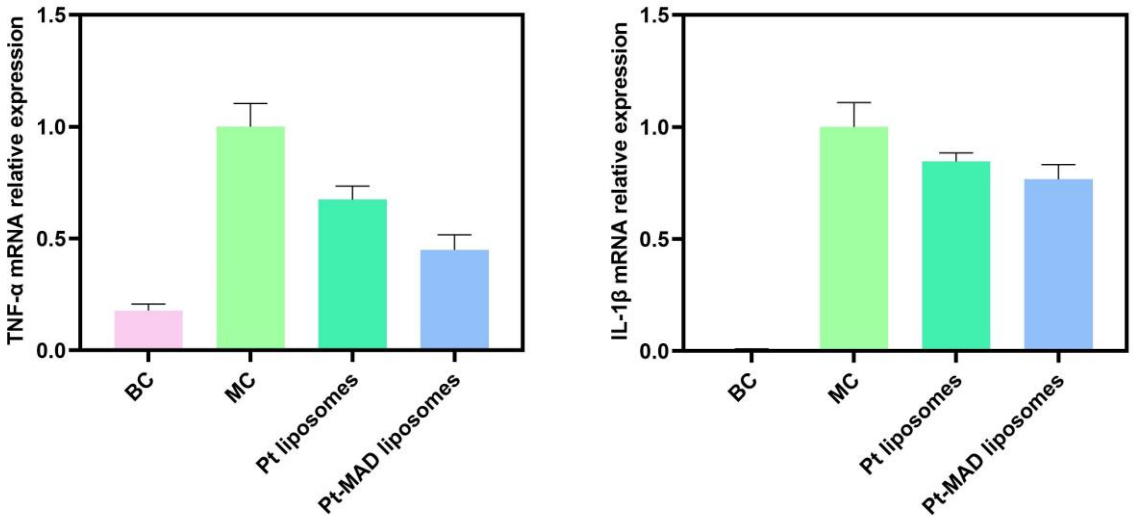

(a) (b)

Figure 6. Effects of the blank control (BC), LPS-induced model control (MC), Pt liposomes, and Pt-MAD liposomes on the mRNA expression of pro-inflammatory cytokines TNF-α (a) and IL-1β (b) in LPS-stimulated THP-1 cells. Data are presented as mean ± SD from replicate experiments. Bar graphs represent relative mRNA expression levels of TNF-α and IL-1β following treatment, as quantified by qPCR.

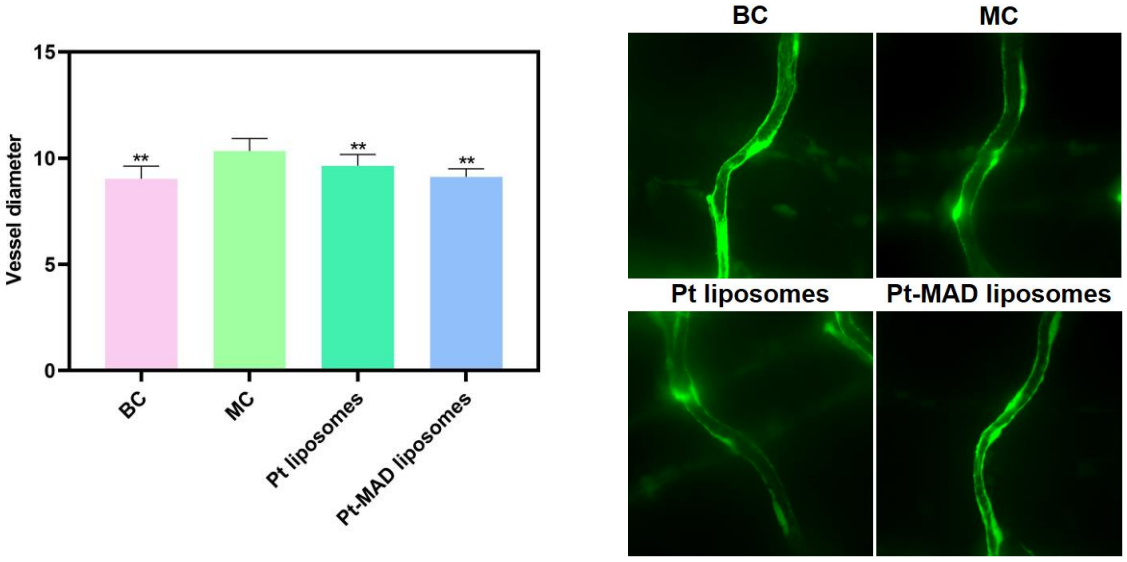

(a) (b)

Figure 7. Statistical analysis of vessel diameters (a) and representative fluorescence images of vascular constriction (b) in zebrafish treated with blank control (BC), model control (MC), Pt liposomes, and Pt-MAD liposomes. The BC group was left untreated, the MC group was exposed to SLS only, and the test groups received SLS in combination with either Pt liposomes or Pt-MAD liposomes. Data are expressed as the mean ± SD from replicate experiments. *$p < 0.05$ and **$p < 0.01$ indicate statistically significant differences compared to the MC group.

3.6. Vasodilation Assay

The diameter of intersegmental blood vessels in transgenic vascular green fluorescent zebrafish (Fli-1) were measured to evaluate the redness-relieving effects of the samples. Zebrafish were assigned to three groups: blank control (BC), model control (MC), and test group. The BC group received no treatment, the MC group was exposed to SLS alone, and the test group was treated with SLS in combination with the liposomal formulations. As shown in Figures 7(a) and 7(b), treatment with 0.05 wt% Pt liposomes and Pt-MAD liposomes significantly reduced vasodilation, indicating effective redness relief. The vessel narrowing (discoloration) rates were 51% for Pt liposomes and 92% for Pt-MAD liposomes. Notably, Pt-MAD liposomes exhibited a more pronounced vasoconstrictive effect, demonstrating a rapid and robust reduction in redness.

3.7. Expression of Inflammatory Factor IL-17

Previous studies have demonstrated that reducing abnormally elevated levels of the inflammatory cytokine IL-17 is beneficial for restoring skin barrier function and maintaining long-term epidermal homeostasis [22]. To evaluate the anti-inflammatory effects of Pt liposomes and Pt-MAD liposomes, a zebrafish injury model was established by exposing the fish to sodium lauryl sulfate (SLS). As shown in Figure 8, the relative expression of IL-17 was significantly upregulated in the MC group following SLS stimulation, confirming the successful establishment of the inflammatory model. Treatment with Pt liposomes and Pt-MAD liposomes significantly decreased IL-17 expression by 26.3% and 53.4%, respectively, compared to the MC group. Notably, Pt-MAD liposomes exerted a more pronounced inhibitory effect, indicating their superior capability to suppress IL-17 expression and restore epidermal barrier balance. These findings suggest that Pt-MAD liposomes may offer a more effective strategy for improving skin barrier function and alleviating inflammation-associated skin disorders [23].

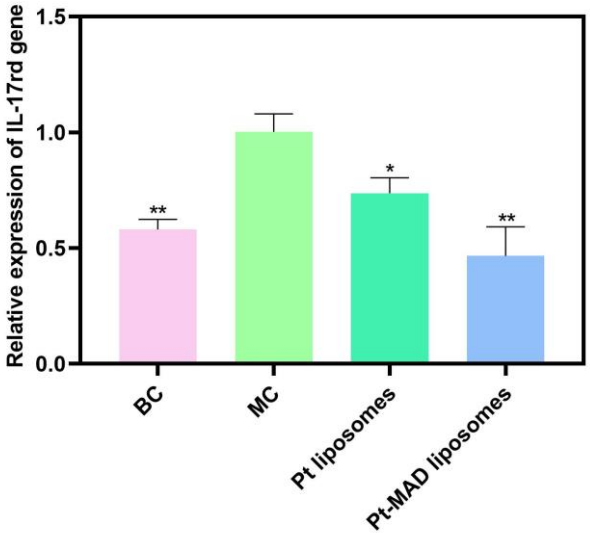

Figure 8. Relative expression of the inflammatory cytokine IL-17 in SLS-stimulated zebrafish treated with blank control (BC), model control (MC), Pt liposomes, and Pt-MAD liposomes. The BC group received no treatment, while the MC group was exposed to SLS only. The test groups were treated with SLS in combination with either Pt liposomes or Pt-MAD liposomes.

IL-17 gene expression was quantified by qPCR. Data are presented as mean ± SD from replicate experiments. *p < 0.05 and **p < 0.01 indicate statistically significant differences compared to the MC group.

4. Discussion

In this study, we successfully developed Pt-MAD liposomes as a targeted delivery system for Pt particles in dermatological applications. AI-driven molecular docking simulations demonstrated that surface functionalization of Pt particles with MAD significantly enhances their binding affinity for five key sensory receptors, suggesting improved targeting and therapeutic potential for sensitive skin-related conditions. These computational findings were strongly supported by experimental data.

Compared to conventional Pt liposomes, Pt-MAD liposomes exhibited markedly superior performance in reducing inflammatory responses, alleviating itch, and mitigating visible skin redness. These effects are likely attributed to the enhanced receptor-binding capacity of the MAD moiety, particularly with dermal sensory receptors such as TRPV1, TRPA1, NK1R, H1R, and ETAR. Furthermore, Pt-MAD liposomes significantly downregulated key inflammatory mediators such as TNF-α and IL-1β. Notably, the marked suppression of IL-17 expression highlights their additional potential to restore epidermal barrier function and maintain long-term skin homeostasis. The integration of MAD as a functional ligand not only enhances the bioavailability of Pt particles but also confers receptor specificity, thereby amplifying therapeutic outcomes. This dual-function design enables more precise interaction with inflammation-related and sensory pathways, which is critical for the management of sensitive skin conditions. Taken together, these findings underscore the potential of Pt-MAD liposomes as a next-generation therapeutic strategy in skincare, offering rapid soothing, enhanced targeting precision, and long-term skin health benefits.

5. Conclusion

At the theoretical level, molecular docking simulations targeting key skin sensory receptors demonstrated that Pt particles functionalized with MAD enabled simultaneous interaction with five critical targets. This suggests enhanced targeting efficiency and faster onset of action compared to unmodified Pt. At the experimental level, In vitro experiments further confirmed that Pt-MAD liposomes outperformed conventional Pt liposomes, validating that the conjugation of the phytodetectoral molecule MAD significantly improved both the speed and efficacy of soothing effects, while also contributing to long-term skin homeostasis.

However, this study still has limitations. The current experiments did not directly verify interactions with the predicted receptor targets, and the precise mechanisms of action remain to be fully elucidated. Future research will focus on investigating the structure–activity relationship between Pt-MAD and additional receptors involved in skin sensitivity, as well as identifying new therapeutic targets. Overall, this study provides a valuable foundation for the development of plant-modified precious metal systems in targeted dermatological applications and cosmetic innovations.

Reference

1. Proksch, E.; Brandner, J.M.; Jensen, J.-M. The skin: an indispensable barrier. *Exp. Dermatol.* **2008**, *17*, 1063-1072.
2. Uehara, Y.; Inoue, T.; Ota, N.; Ikeda, S.; Murase, T. Non-invasive evaluation of subjective sensitive skin by transcriptomics using mRNA in skin surface lipids. *Exp. Dermatol.* **2022**, *31*, 172-181.
3. Willis, C.M.; Shaw, S.; De Lacharrière, O.; Baverel, M.; Reiche, L.; Jourdain, R.; Bastien, P.; Wilkinson, J.D. Sensitive skin: an epidemiological study. *Br. J. Dermatol.* **2001**, *145*, 258-263.
4. Wilzopolski, J.; Kietzmann, M.; Mishra, S.K.; Stark, H.; Bäumer, W.; Rossbach, K. TRPV1 and TRPA1 Channels Are Both Involved Downstream of Histamine-Induced Itch. *Biomolecules* **2021**, *11*.
5. Jang, Y.; Lee, W.J.; Hong, G.S.; Shim, W.S. Red ginseng extract blocks histamine-dependent itch by inhibition of H1R/TRPV1 pathway in sensory neurons. *J. Ginseng Res.* **2015**, *39*, 257-264.
6. Rossbach, K.; Nassenstein, C.; Gschwandtner, M.; Schnell, D.; Sander, K.; Seifert, R.; Stark, H.; Kietzmann, M.; Bäumer, W. Histamine H1, H3 and H4 receptors are involved in pruritus. *Neuroscience* **2011**, *190*, 89-102.
7. Denda, M.; Nakatani, M.; Ikeyama, K.; Tsutsumi, M.; Denda, S. Epidermal keratinocytes as the forefront of the sensory system. *Exp. Dermatol.* **2007**, *16*, 157-161.
8. Raszewska-Famielec, M.; Flieger, J. Nanoparticles for Topical Application in the Treatment of Skin Dysfunctions-An Overview of Dermo-Cosmetic and Dermatological Products. *Int. J. Mol. Sci.* **2022**, *23*.
9. Paiva-Santos, A.C.; Herdade, A.M.; Guerra, C.; Peixoto, D.; Pereira-Silva, M.; Zeinali, M.; Mascarenhas-Melo, F.; Paranhos, A.; Veiga, F. Plant-mediated green synthesis of metal-based nanoparticles for dermopharmaceutical and cosmetic applications. *Int. J. Pharm.* **2021**, *597*.
10. Yoshihisa, Y.; Honda, A.; Zhao, Q.L.; Makino, T.; Abe, R.; Matsui, K.; Shimizu, H.; Miyamoto, Y.; Kondo, T.; Shimizu, T. Protective effects of platinum nanoparticles against UV-light-induced epidermal inflammation. *Exp. Dermatol.* **2010**, *19*, 1000-1006.
11. Liu, J.B.; Jiang, X.M.; Wang, L.M.; Hu, Z.J.; Wen, T.; Liu, W.Q.; Yin, J.J.; Chen, C.Y.; Wu, X.C. Ferroxidase-like activity of Au nanorod/Pt nanodot structures and implications for cellular oxidative stress. *Nano Res.* **2015**, *8*, 4024-4037.
12. Koczkur, K.M.; Mourdikoudis, S.; Polavarapu, L.; Skrabalak, S.E. Polyvinylpyrrolidone (PVP) in nanoparticle synthesis. *Dalton Trans.* **2015**, *44*, 17883-17905.
13. Ahmad, F.; Salem-Bekhit, M.M.; Khan, F.; Alshehri, S.; Khan, A.; Ghoneim, M.M.; Wu, H.-F.; Taha, E.I.; Elbagory, I. Unique Properties of Surface-Functionalized Nanoparticles for Bio-Application: Functionalization Mechanisms and Importance in Application. *Nanomater.* **2022**, *12*, 1333.
14. Nellore, J.; Pauline, C.; Amarnath, K. Bacopa monnieri Phytochemicals Mediated Synthesis of Platinum Nanoparticles and Its Neurorescue Effect on 1-Methyl 4-Phenyl 1,2,3,6 Tetrahydropyridine-Induced Experimental Parkinsonism in Zebrafish. *J. Neurodegener. Dis.* **2013**, *2013*, 972391.
15. Teow, Y.; Valiyaveettil, S. Active targeting of cancer cells using folic acid-conjugated platinum nanoparticles. *Nanoscale* **2010**, *2*, 2607-2613.

16. Ma, Z.Y.; Zhang, Y.F.; Zhang, J.; Zhang, W.Y.; Foda, M.F.; Dai, X.X.; Han, H.Y. Ultrasmall Peptide-Coated Platinum Nanoparticles for Precise NIR-II Photothermal Therapy by Mitochondrial Targeting. *ACS Appl. Mater. Interfaces* **2020**, *12*, 39434-39443.
17. Puttarak, P.; Panichayupakaranant, P. Factors affecting the content of pentacyclic triterpenes in Centella asiatica raw materials. *Pharm. Biol.* **2012**, *50*, 1508-1512.
18. Fu, X.J.; He, S.J.; Wang, L.; Xue, Y.Y.; Qiao, S.G.; An, J.Z.; Xia, T.T. Madecassic Acid Ameliorates the Progression of Osteoarthritis: An in vitro and in vivo Study. *Drug Des. Devel. Ther.* **2022**, *16*, 3793-3804.
19. Solá, P.; Mereu, E.; Bonjoch, J.; Casado-Peláez, M.; Prats, N.; Aguilera, M.; Reina, O.; Blanco, E.; Esteller, M.; Di Croce, L.; et al. Targeting lymphoid-derived IL-17 signaling to delay skin aging. *Nat. Aging* **2023**, *3*, 688-704.
20. Chen, J.W.; Sun, W.Q.; Zhu, Y.J.; Zhao, F.; Deng, S.X.; Tian, M.; Wang, Y.; Gong, Y. TRPV1: The key bridge in neuroimmune interactions. *J. Intensive Med.* **2024**, *4*, 442-452.
21. Bagood, M.D.; Isseroff, R.R. TRPV1: Role in Skin and Skin Diseases and Potential Target for Improving Wound Healing. *Int. J. Mol. Sci.* **2021**, *22*.
22. Brembilla, N.C.; Senra, L.; Boehncke, W.H. The IL-17 Family of Cytokines in Psoriasis: IL-17A and Beyond. *Front. Immunol.* **2018**, *9*.
23. Gutowska-Owsiak, D.; Schaupp, A.L.; Salimi, M.; Selvakumar, T.A.; McPherson, T.; Taylor, S.; Ogg, G.S. IL-17 downregulates filaggrin and affects keratinocyte expression of genes associated with cellular adhesion. *Exp. Dermatol.* **2012**, *21*, 104-110.